

RESEARCH

Open Access



Outage performance and energy efficiency optimization of wireless-powered millimeter-wave sensor networks

Xiaowu Li¹, Fuan Xiao², Kun Tang^{3*}  and Entao Luo²

*Correspondence:
tangkun@scut.edu.cn

¹ College of Science, Hunan University of Science and Engineering, No. 130, Yangzitan Road, Yongzhou City 425000, China

² School of Information Engineering, Hunan University of Science and Engineering, No. 130, Yangzitan Road, Yongzhou City 425000, China

³ Guangdong Provincial Key Laboratory of Millimeter Wave and Terahertz, School of Electronic and Information Engineering, South China University of Technology, No. 381, Wushan Road, Guangzhou City 510641, China

Abstract

With the widespread use of wireless sensor networks, one of the most pressing concerns is extending the lifetime of the sensors. By deploying directional antenna arrays, millimeter wave (mmWave) is a possible candidate for wireless energy transfer (WPT). This paper investigates a beneficial combination of WPT and data transmission in a typical mmWave sensor network with Rayleigh channels, where a transmission interval can be divided into two sub-intervals. During the first sub-interval, one hybrid access point (HAP) employs beamforming techniques to transfer energy for serving multiple sensors within the service sector. The sensors then transmit their individual signal in turn to the HAP based on time division multiple address (TDMA) strategy by using the whole harvested energy. According to stochastic geometry, the exact and approximate expressions of beam outage probability for the considered system are determined, respectively. The optimal time allocation of energy harvesting and data transmission for sensors is examined in order to maximize the energy efficiency of the system. The optimization problem can be translated into corresponding parametric form, and the resulting optimization problem can be solved using the Lagrange dual method with Karush–Kuhn–Tucker (KKT) conditions. The numerical results show the variation trend of the beam outage probability under various parameters and verify the accuracy of the theoretical analyses. Furthermore, the simulation results illustrate that the proposed optimal time allocation strategy can significantly enhance the overall energy efficiency of the system compared with a similar scheme.

Keywords: Wireless sensor networks, Millimeter-wave, Wireless power transfer, Optimal time allocation, Energy efficiency

1 Introduction

Many different types of wireless sensor networks (WSNs) have been deployed in recent years, while more WSNs and sensor devices will take their places, which will be a decisive step towards building a large-scale Internet of Things (IoT). However, the limited lifetime of sensor devices is still one of the major limitations of WSNs [1]. Fortunately, recent advances in ultra-low power signal processing and wireless communications can provide a variety of solutions to this challenge. For example, sensors can use wireless energy harvesting techniques to convert other ambient energy into electricity, so that

the sensor can receive a continuous power supply without having to replace the battery [2, 3]. Although solar energy, kinetic energy, and floor vibration can be used to power the sensors, the dynamic nature of these resources, as well as a lack of prior knowledge of energy distribution will bring great difficulties to the protocol design of the systems. In contrast, harvesting energy from ambient radio frequency (RF) signals presents a potentially more efficient approach owing to its wireless nature, ready availability, low cost, and the feasibility of small form factor implementation [4]. This method proves particularly suitable for wireless energy transfer (WPT) applications in scenarios such as smart homes, forest fire monitoring, and indoor IoT systems [5–7]. With the growing demand of RF energy harvesting, commercialized products, such as Powercaster and Cota systems have been entered the market [8].

Although WPT techniques promise tremendous benefits, some key challenges must be resolved before they are deployed in the WSNs. Firstly, because the great attenuation of the electromagnetic waves with the increase of distance, only a portion of the energy radiated by an energy transmitter can be harvested by an energy receiver [9]. Secondly, in WPT, the sensitivity of the current energy receivers is as high as -10 dBm, while the sensitivity of the information receiver is only -60 dBm [10]. At present, there are three main approaches to solve the above problems: *i*) forming the RF energy into narrow beams; *ii*) keeping the distance between transmitter and receiver as smaller as possible in the design of network architecture; *iii*) adopting massive MIMO technique to enhance spectral efficiency and energy efficiency (EE) [11].

In the fifth-generation (5G) communications, the implementation of cost-effective, low-power, and ultra-dense cell systems has the potential to enhance network performance in terms of energy efficiency and load balancing. Due to the physical properties of mmWave communication, i.e., a frequency band ranging from 30 to 300 GHz and corresponding wavelengths from 10 to 1 mm [12], mmWave technology can leverage larger quantities of available spectrum. Additionally, it can utilize massive antenna arrays to facilitate highly directional transmission and reception. This capability is achievable at higher frequencies owing to the smaller size of antenna components [13]. Furthermore, mmWave communications can be realized in the range of 150–200 m in the urban environments [14]. As a result, mmWave is considered as the prime candidate for 5G systems, while mmWave can offer all three solutions to enhance WPT performance [15]. Therefore, the above factors ensure the availability and feasibility of WPT by mmWave in 5G networks.

1.1 Related work

In communication systems, WPT can be realized by utilizing the following two architectures, i.e., wireless-powered communication networks (WPCNs) and simultaneous wireless information and power transfer (SWIPT) [16, 17]. For WPCNs, the harvest-then-transmit (HTT) protocol was proposed with a general multi-user wireless-powered interference channel in [18], where the communication time is divided into two phases, i.e., wireless energy harvesting (WEH) and wireless information transmission (WIT). The key of SWIPT is that both information and energy can be extracted simultaneously from the same received RF signals via time-switching (TS) scheme or power-splitting (PS) scheme [19]. Two SWIPT cooperative spectrum sharing strategies were proposed

aiming to improve the spectral and energy efficiencies for cognitive IoT networks in 6G communication systems, where IoT devices can harvest energy from RF signals and can be acted as orthogonal frequency division multiple (OFDM) relay to access the primary spectrum [20]. Multicast communication of a satellite and aerial-integrated network with rate-splitting multiple access was investigated to satisfy the demands of massive IoT devices accessing [21].

At present, a large number of WPT related studies have been carried out in microwave networks (below 6 GHz). In [22], the authors developed a WPT-based WIT scheme in relay-based CRNs, where a secondary network can share the spectrum and harvest energy to assist the data transmission of the primary network. The authors in [23] considered a multiple relay-assisted cooperative cognitive radio system, where the relays first harvested RF energy from the primary transmitter and then adopted decode-and-forward (DF) method to transmit data. In addition, three best relay selection schemes were also investigated. The authors of [24] considered a two-way amplify-and-forward (AF) relay network, where two nodes exchange information with assistance of an energy harvesting MIMO relay. The authors further optimized the power allocation ratios, precoding matrix, and RF phase shifting factor to maximize the sum-rate of the considered network [25]. investigated the wireless-powered relay network with harvest-receive-forward time-switching scheme, where the relay can random harvest RF energy from dedicated energy signal and other ambient resources. The maximal offline throughput in different scenarios was considered by optimizing the time fraction and reception rate. A novel architecture design for the green WSNs in smart cities was considered in [26], where an efficient energy and information transfer protocol was proposed to enhance the performance of transmission rate. In addition, beamforming design is other key factor for WEH and WIT. In [11], the authors considered a hybrid satellite-terrestrial relay network to optimally joint design beamforming vectors. The authors of [27] proposed a joint optimization design for a NOMA-based satellite-terrestrial integrated networks, which can share the mmWave spectrum with a cellular network.

Although the research on mmWave communications and related topics have been extensive, the investigation on the combination of mmWave and WPT is still limited. The authors of [28] proposed an analytical framework to investigate capability of mmWave WPT with large-scale antennas, i.e., energy coverage probability, average harvested energy, and achievable rate, by utilizing stochastic geometry method. In [29], the authors analyzed the performance of WPT in a large-scale mmWave tactical network, in which a person equipped with WEH nodes were powered by another person equipped with power beacon (PB) nodes. Taking human as potential blockages, the energy coverage probability and overall success probability were derived. A directional power transfer scheme based on beamforming was proposed in [30] for a large-scale network, where each PB can steer its beam toward the direction with maximum receiving power during the training phase. The aforementioned architectures for microwave networks have been investigated in the area of mmWave communications. A SWPIT-enabled mmWave network is considered in [31]. A corresponding optimal PS scheme was proposed to improve the system performance in terms of reducing communication interruption and information loss. The authors in [32] considered a mmWave MIMO-NOMA system with SWIPT and studied maximizing the achievable sum-rate and total

energy efficiency. Furthermore, the secrecy performance of SWIPT-enabled mmWave ultra-dense networks was investigated with a stochastic geometry framework [33]. In order to both improve the system security and reduce energy consumption, the authors in [34] proposed an alternative optimization algorithm to address the problem. In [35], the authors represented a secrecy-energy efficient hybrid beamforming design for mmWave-based satellite-terrestrial integrated network, where the sub-optimal solutions with two robust beamforming schemes were obtained to solve the considered optimization problem. Moreover, the multibeam satellite system with secure energy efficient beamforming was investigated in [36], where an alternating optimization scheme was applied to address the secrecy energy efficiency problem.

1.2 Motivation and contribution

With the further development of 5G technologies, IoT systems based on mmWave sensor networks will be implemented everywhere. This paper investigates a typical mmWave sensor network where each sensor can harvest RF energy in downlink and then use the harvested energy for data transmission in uplink. This model can provide an effective solution for sensors that are inconvenient for battery replacement or continuous power supply in IoT systems, such as intelligent transportation systems and human data monitoring. Unlike [31, 32], which either only focuses on deriving close-form expressions of system performance or only optimizes the energy efficiency of the system. In order to further study the wireless-powered mmWave sensor networks, we first theoretically analyze the system performance, which aims to derive the closed-form solution of the beam outage probability within a stochastic geometry framework random in uplink after the sensors harvest RF energy in downlink. Then, according to the proposed transmission protocol, the transmission slots in downlink and uplink are jointly optimized to guarantee the maximum energy efficiency in uplink. The main contributions can be summarized as follows:

- We investigate a wireless-powered mmWave sensor network within a cellular, in which the hybrid access point (HAP) is located at the central point of the cellular network and the sensors are spatially distributed around it. The HTT protocol is adopted, where the whole transmission slot is divided into two sub-slots. In the first sub-slot, the HAP transmits RF energy signal to multiple sensors through the downlink. In the second sub-slot, these sensors use the harvested energy to transmit their individual signals to the HAP under the TDMA mode. According to the proposed transmission protocol, an analytical expression of the system beam outage probability is derived by using stochastic geometry theory. In the meanwhile, for two special cases, the approximate closed expressions of the system beam outage probability are further derived.
- In order to maximize the energy efficiency of the system, it can be achieved by optimizing the transmission slot allocations of WPT in downlink and WIT in uplink. Therefore, we propose a corresponding optimization problem, which can be converted into its parametric form. Then, the new formed optimization problem can be solved by adopting the Lagrange dual multipliers method with corresponding

KKT conditions. Finally, the Dinkelbach algorithm is adopted to iteratively obtain the global optimal timeslot allocation.

The numerical results provide useful insights that the beam outage probability of the considered system is significantly impacted by various parameters, such as central angle of service sector, the number of antennas, fading severity parameters, density of homogeneous Poisson point process (HPPP), etc. Moreover, the simulation results also reveal that the proposed algorithm for optimal timeslot allocation can effectively improve the performance of the system compared to the corresponding ergodic analyses in terms of energy efficiency and sum achievable rate.

The rest of this paper is organized as follows. In Section II, network topology, channel model, and transmission protocol are presented. Section III derives the beam outage probability of the system and optimal time allocation algorithm is also proposed in this section. Section IV contains simulation results. Section V summarizes this paper.

2 Methods/experimental

In this paper, we mainly study the outage probability when the signal is transmitted by energy-constrained sensors in a wireless-powered millimeter-wave sensor network (WP-MWSN), and optimize the downlink and uplink transmission slot allocation to improve the EE of sensors in uplink transmission. The beam outage probability is calculated by obtaining the cumulative distribution function (CDF) of the achievable rate at the sensor. Then, by constructing the Lagrange function corresponding to the optimization problem and the KKT condition, Dinkelbach algorithm is utilized to iteratively obtain the optimal allocations of downlink and uplink transmission slots. Finally, Matlab simulation is used to demonstrate the performance of the derived outage probability and verify whether it matches with the corresponding Monte Carlo simulation. In addition, Matlab simulation is further used to verify the advantages of optimized downlink and uplink slot allocation in improving the EE of the system.

3 System model

3.1 Network topology

As shown in Fig. 1, we consider a wireless-powered millimeter-wave sensor network (WP-MWSN) consisting of one HAP and multiple randomly deployed sensors in a single cell, which is modeled as a disc with radius R . The HAP is plugged into a constant power

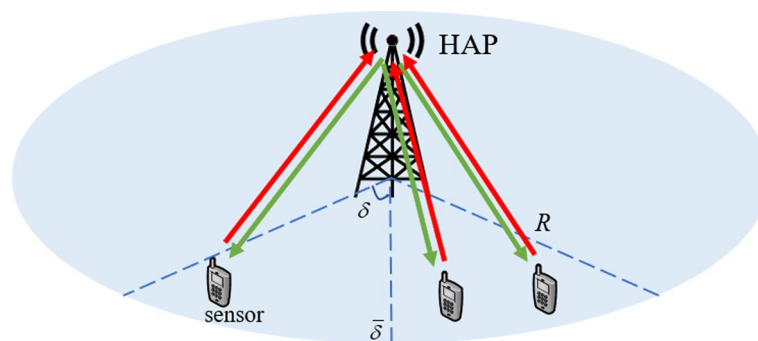


Fig. 1 The considered system model of wireless-powered millimeter-wave sensor networks (WP-MWSN)

supply and equipped with a uniform linear array of M antennas. All sensors harvest energy from the HAP's transmitted energy signals and equipped with a small mmWave antenna array, where several power dividers are used to combine sub-arrays into one channel for signal reception and transmission [37]. As a result, the small antenna array on the sensor can be regarded as an antenna unit. We assume that the HAP is located at the origin of the disc. The spatial distribution of sensors is followed as a homogeneous Poisson point process (HPPP) $\Phi=\{x_k\}, k \geq 1$, in Euclidean plane with density λ , where x_k is defined as the coordinates of the k -th sensor.

The protocol on harvest-then-transmit (HTT) is followed in this paper. According to the TDMA scheme, each transmission interval T is divided into two sub-intervals for downlink and uplink, respectively. Sensors first preform WEH in the downlink and then send data in the uplink towards WIT. The received noise at all receivers is additive white Gaussian noise (AWGN) with zero mean and average power σ_0^2 .

3.2 Channel model

Measurement findings showed that mmWave links undergo different channel conditions, which are characterized by a line of sight (LOS) link and several non-line of sight (NLOS) links [38]. Therefore, the mmWave link between the HAP and k -th sensor can be modeled as

$$\mathbf{h}_k = \frac{g_{k,L}\sqrt{M}\mathbf{a}(\delta_{k,L})}{\sqrt{1+d_k^{\beta_L}}} + \sqrt{M}\sum_{l=1}^L \frac{g_{k,NL}^l\mathbf{a}(\delta_{k,NL}^l)}{\sqrt{1+d_k^{\beta_{NL}}}}, \tag{1}$$

where $g_{k,L}$ and $\delta_{k,L}$ denote the complex gain and normalized direction of the link with k -th sensor for LOS path, respectively; $g_{k,NL}$ and $\delta_{k,NL}$ represent the complex gain and normalized direction of the link with k -th sensor for NLOS path, respectively; β_L and β_{NL} represent the path-loss exponents for LOS path and NLOS path, respectively; d_k represents the Euclidean distance from the HAP to the k -th sensor. In addition, $\mathbf{a}(\delta_k)$ is the array steering vector, which can be expressed as

$$\mathbf{a}(\delta_k) = \frac{1}{\sqrt{M}} \left(1, e^{-i\pi\delta_k}, \dots, e^{-i\pi(M-1)\delta_k} \right)^T, \tag{2}$$

where $(\cdot)^T$ indicates the transpose of matrix, $\delta_k=2d \sin(\phi_k)/\omega$ denotes the normalized direction of the LOS link with the k -th sensor, where $\phi_k \in [-\pi/2, \pi/2]$ is the physical angle of the k -th sensor, d and ω denote the distance between two adjacent antennas and the carrier wavelength, respectively.

Furthermore, each mmWave channel has different propagation property since it characterized by a strong LOS link as if in free space and several weak NLOS links. In the mmWave channel, the path-loss of NLOS component is much larger than the path-loss of LOS component, which because that the power of $g_{k,L}$ associated with NLOS link is lower 20 dB than the complex gain associated with LOS link [39]. Therefore, the effect of NLOS links can be neglected, i.e., $g_{k,NL}^l = 0, \forall l$, and only LOS component is considered for mmWave links. The mmWave channel response of the link between the HAP and k -th sensor can be simplified as

$$\mathbf{h}_k = \frac{g_k \sqrt{M}}{\sqrt{1 + d_k^\beta}} \mathbf{a}(\delta_k), \tag{3}$$

where g_k and δ_k represent the complex gain and normalized direction of the link with k -th sensor for LOS path, respectively, with g_k assuming to be a complex normal random variable, i.e., $g_k \sim CN(0, 1)$. It should be noted that the analytical method in this paper can be used to analyze the outage performance of NLOS user, where the probability density function (PDF) of the channel gain between the HAP and NLOS user, and then substituting it into the expression.

3.3 Energy harvesting and information transmission

Based on the HTT protocol, the whole transmission interval T can be divided into WEH and WIT sub-intervals, which is shown in Fig. 2. Assuming K sensors existed in the service sector, all sensors first harvest energy in the downlink during the WEH sub-interval, then the WIT sub-interval of uplink is divided into K slots and all sensors transmit their individual signal to HAP with TDMA mode by utilizing the whole harvested energy of each sensor.

During WEH sub-interval $\alpha_0 T$, HAP sends energy beamforming vector to serve multiple sensors with a normalized direction $\bar{\delta}$. The energy beam is given by

$$\mathbf{v} = \mathbf{a}(\bar{\delta}), \tag{4}$$

where $\mathbf{a}(\bar{\delta})$ can be obtained from (2) with $\bar{\delta}$ being distributed uniformly in normalized direction in $[-1, 1]$. As shown in Fig. 1, the sensors are located in the fan-shaped sector with normalized direction $\bar{\delta}$ with central angle 2δ , which can be obtain through a low-complexity training process or the Global Positioning System (GPS). Then, the effective channel gain of the k -th sensor is given by

$$|\mathbf{h}_k^H \mathbf{v}|^2 = \frac{|g_k|^2 F_M(\bar{\delta} - \delta_k)}{1 + d_k^\beta}, \tag{5}$$

where

$$F_M(\bar{\delta} - \delta_k) = \frac{\sin^2\left(\frac{\pi M(\bar{\delta} - \delta_k)}{2}\right)}{M \sin^2\left(\frac{\pi(\bar{\delta} - \delta_k)}{2}\right)} \tag{6}$$

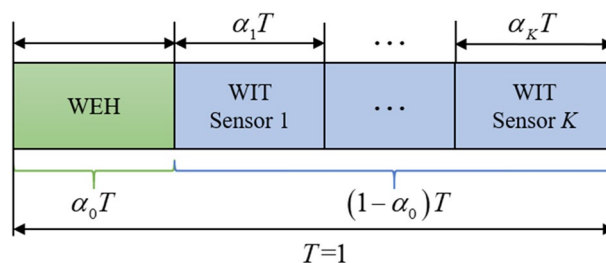


Fig. 2 Frame structure of TDMA-based HTT protocol for the considered WP-MWSN

denotes the Fejér kernel [40]. To simplify the analysis, we set $\bar{\delta}=0$ and the received RF power at the k -th sensor can be expressed as

$$P_k^{\text{RF}} = P_{\text{HAP}} |\mathbf{h}_k^H \mathbf{v}|^2 = \frac{P_{\text{HAP}} |g_k|^2}{1 + d_k^\beta} F_M(\delta_k), \tag{7}$$

where P_{HAP} is constant transmit power of the HAP. Then, the amount of harvested energy at the k -th sensor based on the linear WEH model can be calculated as

$$E_k = \alpha_0 T \eta P_k^{\text{RF}} = \frac{\alpha_0 T \eta P_{\text{HAP}} |g_k|^2}{1 + d_k^\beta} F_M(\delta_k), \tag{8}$$

where $\eta \in (0, 1]$ represents the energy conversion efficiency. The harvested energy from the AWGN is negligible. Note that many studies focus on non-linear WEH since it can better reflect the saturation effect of energy harvesting. However, we consider the low-power mmWave communication systems, in which the transmit power of mmWave base station is relatively low, so the rectification process can be approximately expressed as linear [41]. Therefore, linear WEH model is adopted in this paper.

During the WIT sub-interval $(1 - \alpha_0)T$, with the specified time-slot, K sensors will transfer information to HAP using all harvested energy with TDMA mode. As a result, the achievable throughput of the k -th sensor at the HAP is given by

$$v_k = \alpha_k T \log_2 \left(1 + \frac{E_k |\mathbf{h}_k^H \mathbf{v}|^2}{\alpha_k T \sigma_0^2} \right) = \alpha_k T \log_2 \left(1 + \frac{E_k |g'_k|^2 F_M(\delta_k)}{\alpha_k T \sigma_0^2 (1 + d_k^\beta)} \right), \tag{9}$$

where $\alpha_k T$ denotes the allocated time duration of WIT for the k -th sensor, \mathbf{h}'_k and g'_k are the channel and complex gain between the k -th sensor and HAP, respectively.

4 Beam outage probability and optimal time allocation

In this section, we commence with an analysis of the beam outage probability within the considered system. Subsequently, we determine the optimal time allocation for WEH and WIT involving K sensors. The focus of this analysis is on a representative sensor within the service sector; thus, for the sake of simplicity in description, we omit the subscripts used in the previous section. Throughout the following discussions, we set $T=1$. To facilitate a clearer expression of the beam outage probability, we establish a scenario where the transmission duration in the uplink for each user is identical. This choice is motivated by the difficulty in obtaining the probability density function for any arbitrary timeslot assignment.

4.1 Beam outage probability

The outage probability is a vital performance measure to characterize the performance of wireless networks. Mathematically, the beam outage probability is defined as the probability that the achievable rate of a sensor is below a given threshold r . In order to insight the closed-form expression of the beam outage probability for the considered system, we simplify to set that the remaining WIT duration is divided equally for the K sensors. It should be noted that if the sub-timeslot allocation of each

sensor is different, then the probability density function (PDF) of the sub-timeslot allocation needs to be obtained in advance for calculating the exactly expression of beam outage probability. Since the optimization goal of the system needs to be determined according to the actual application, the PDF of sub-timeslot allocation is difficult to obtain. Thus, we equally divided the uplink transmission timeslot for each sensor. Considering K sensors located at the service sector to transmit their individual signal to the HAP, the expression of beam outage probability is given by

$$P_{\text{out}} = \Pr \left\{ \frac{(1 - \alpha_0)}{K} \log_2 \left(1 + \frac{KE|\mathbf{h}^H \mathbf{v}|^2}{(1 - \alpha_0)\sigma_0^2} \right) < r|K \right\}, \quad (10)$$

where r denotes the target transmission rate. In order to derive the closed-form expression of (10), we first derive the cumulative distribution function (CDF) of a typical sensor's achievable rate, which is shown as the following Lemma.

Lemma 1: Assume there are K sensors within the service sector, the CDF of achievable rate for a typical sensor at the HAP can be expressed as

$$F_{AR}(r) = 1 - \frac{1}{\delta R^2} \int_{-\delta}^{\delta} \int_0^R \exp \left(-\frac{A(1 + r^\beta)}{\Omega F_M(\phi)} \right) r dr d\phi, \quad (11)$$

where $A = \sqrt{(1 - \alpha_0)\sigma_0^2 [2^{rK/(1-\alpha_0)} - 1]} / (K\alpha_0\eta P_{\text{HAP}})$.

Proof: Please refer to Appendix.

It should be noted that it is difficult to obtain the closed-form expression of (11) since an integral part existed. In order to obtain further insights from Lemma 1, we simplify some components of the derived expression to obtain approximate results of (11) as follows:

1) *Special Case 1:* This case corresponds to a high SNR scenario with a small number of sensors, i.e., $K \rightarrow \infty$, the SNR of transmit power for HAP is high. Then, we have $A \rightarrow 0$. On the basis of the fact that $\exp(-y) \approx 1 - y$ for $y \rightarrow 0$, (11) can be rewritten as

$$\begin{aligned} F_{AR}(r) &\approx 1 - \frac{1}{\delta R^2} \int_{-\delta}^{\delta} \int_0^R \left(1 - \frac{A(1 + r^\beta)}{\Omega F_M(\phi)} \right) r dr d\phi \\ &= \frac{A}{\Omega \delta R^2} \int_{-\delta}^{\delta} \frac{1}{F_M(\phi)} d\phi \int_0^R (1 + r^\beta) r dr \\ &= \left[\frac{A}{2\Omega \delta} + \frac{AR^\beta}{\Omega \delta (\beta + 2)} \right] \int_{-\delta}^{\delta} \frac{1}{F_M(\phi)} d\phi. \end{aligned} \quad (12)$$

2) *Special Case 2:* In this case, in addition to considering the case of high SNR and small number of sensors, we also consider the case where the central angle 2δ of service sector is small, i.e., $\delta \rightarrow 0$. Since $\sin(y) \approx y$ for $y \rightarrow 0$ and $\text{sinc}(y) = \sin(y)/y$, we can get $F_M(\phi) \approx M \text{sinc}(\pi \phi M/2)$. Furthermore, based on the fact that $\text{sinc}(y) \approx 1 - y^2/6$ and $(1 - y)^2 \approx 1 - 2y$ for $y \rightarrow 0$, the Fejér kernel can be approximately expressed as

$$F_M(\phi) \approx M \left[1 - \frac{(\pi M \phi)^2}{12} \right]. \tag{13}$$

Substituting (13) into (12) and utilizing the fact that $(1 - y)^{-1} \approx 1 + y$ for $y \rightarrow 0$, the result of (12) can be further approximated as

$$F_{AR}(w) \approx \frac{2}{M} \left[\frac{A}{2\Omega} + \frac{AR^\beta}{\Omega(\beta + 2)} \right] \left(1 + \frac{\pi^2 M^2 \delta^2}{36} \right). \tag{14}$$

Then, the beam outage probability is shown as following proposition.

Proposition 1: *Suppose there are K sensors within the service sector, the beam outage probability for the considered system is given by.*

$$P_{out} = \sum_{K=1}^{\infty} \frac{\mu^K \exp(-\mu)}{K!} F_{AR} \left(2^{\frac{rK}{1-\alpha_0}} - 1 \right), \tag{15}$$

where $\mu = \lambda \delta \pi R^2$ is the area of the service sector with central angle 2δ , $F_{AR}(\cdot)$ is given in (11).

Proof: From Lemma 1, (10) can be rewritten as.

$$P_{out} = \Pr \{ v < r|K \} = E \left\{ F_{AR} \left(2^{\frac{rK}{1-\alpha_0}} - 1 \right) \right\}. \tag{16}$$

Then, the probability that the area of the service sector with density λ contains K sensors is given as $\mu^K \exp(-\mu)/K!$ [42]. By taking the expectation with respect to the amount of sensors K , the proposition can be proved.

4.2 Optimal time allocation

When the system beam outage probability is analyzed above, the transmission timeslot in uplink is evenly divided to each sensor for convenience of calculation. However, in practical applications, uplink sub-timeslots can be allocated more reasonably according to different application requirements. In order to further study how to improve the system performance, we aim to maximize the energy efficiency (EE) of the system, and realize the efficient green communications by optimizing the allocations of WET sub-timeslot in downlink and WIT sub-timeslots based on TDMA operation. Therefore, we aim to maximize the EE of the considered system by optimizing the allocation of WIT sub-intervals for sensors in the service sector. The EE is defined as

$$EE = \frac{R_{sum}}{E_T}, \tag{17}$$

where R_{sum} and E_T denote the system throughput with K sensors and total energy consumption, respectively, which are given by

$$R_{sum} = \sum_{k=1}^K \alpha_k \log_2 \left(1 + \frac{\alpha_0}{\alpha_k} B_k \right), \tag{18}$$

$$E_T = \sum_{k=1}^K \alpha_0 C_k, \tag{19}$$

with $B_k = \frac{\eta^{P_{\text{HAP}}} |g_k|^4}{\sigma_0^2 (1+d_k^\beta)^2} F_M^2(\delta_k)$ and $C_k = \frac{\eta^{P_{\text{HAP}}} |g_k|^2}{1+d_k^\beta} F_M(\delta_k)$. Note that in the TDMA mode, the

HAP can rely on channel reciprocity to acquire full CSI of uplink when the uplink and downlink share the same band [43]. According to the channel reciprocity, the result of effective complex gain for uplink $|g'_k|^2$ in (9) is equal to $|g_k|^2$.

In order to maximize the EE, the optimization problem can be equivalently given by (P1) based on (17), (18), and (19).

$$\begin{aligned} & \max_{\alpha_0, \{\alpha_k\}} EE \\ & \text{s.t. C1: } \alpha_0 + \sum_{k=1}^K \alpha_k \leq T, \\ & \text{C2: } \alpha_0 > 0, \alpha_k \geq 0. \end{aligned} \tag{20}$$

In (20), α_0 and $\{\alpha_k\}$ represent the downlink energy transmission duration and uplink data transmission duration for each sensor, respectively. Therefore, the constraint C1 in (20) indicates that the sum of α_0 and $\{\alpha_k\}$ is less than or equal to a whole transmission interval. In the constraint C2, we set $\alpha_0 > 0$ and $\alpha_k \geq 0$, where $\alpha_k = 0$ occurs when the k -th sensor does not harvest RF energy. To obtain the optimal pair of $(\alpha_0, \{\alpha_k\})$, we first prove that the objective function in (20) is a concave function. Since the constraint C1 $\alpha_0 + \sum_{k=1}^K \alpha_k \leq T$ illustrating the parameters between the α_0 and $\{\alpha_k\}$ are coupled, we thus need to the concavity of the subject function when α_0 is fixed. Correspondingly, the second derivative of the subjective function can be equivalently expressed as

$$\begin{aligned} f''(\alpha_k) &= \left(\alpha_k \log_2 \left(1 + \frac{\alpha_0}{\alpha_k} B_k \right) \right)'' \\ &= - \frac{\alpha_0^2 B_k^2}{\alpha_k^3 + 2\alpha_0 B_k \alpha_k^2 + \alpha_0^2 B_k^2 \alpha_k} < 0, \end{aligned} \tag{21}$$

which means that optimization problem (P1) is actually a concave optimization problem [44]. Therefore, the optimal solution can be obtained by transferring the objective function in (P1) into parametric form and then adopting the Lagrange dual multipliers method. The parametric form of objective function in optimization problem (P1) can be rewritten as

$$F(\theta) = \max_{\alpha_0, \{\alpha_k\}} R_{\text{sum}} - \theta E_T, \tag{22}$$

where θ denotes a non-negative parameter. For a given θ , the Lagrangian function of optimization problem (P1) is given by

$$\begin{aligned}
 L(\alpha_0, \{\alpha_k\}) &= \sum_{k=1}^K \left[\alpha_k \log_2 \left(1 + \frac{\alpha_0 B_k}{\alpha_k} \right) - \theta \alpha_0 C_k \right] \\
 &+ \xi \left[T - \alpha_0 - \sum_{k=1}^K \alpha_k \right],
 \end{aligned} \tag{23}$$

where ξ is Lagrangian coefficient. Based on the complementary slackness, the optimal lagrange multipliers are zero for constrain C2. We thus omit the corresponding lagrangian multipliers in (23). According to the KKT conditions of lagrangian function (23), we have

$$\frac{\partial L}{\partial \alpha_0} = \sum_{k=1}^K \left[\frac{B_k \log_2(e)}{B_k \alpha_0 / \alpha_k + 1} - \theta C_k \right] - \xi = 0, \tag{24}$$

$$\frac{\partial L}{\partial \alpha_k} = \left[\log_2 \left(1 + \frac{\alpha_0 B_k}{\alpha_k} \right) - \left(\frac{B_k}{1 + B_k \alpha_0 / \alpha_k} \frac{\alpha_0}{\alpha_k} \right) \log_2(e) \right] - \xi = 0, \tag{25}$$

$$\xi \left(T - \alpha_0 - \sum_{k=1}^K \alpha_k \right) = 0, \tag{26}$$

respectively. From (25), result of ξ can be obtained and then substituting it into (24), we have

$$\begin{aligned}
 &\sum_{k=1}^K \left[\frac{B_k \log_2(e)}{B_k \Delta_k + 1} - \theta C_k \right] - \log_2(1 + B_k \Delta_k) \\
 &+ \left(\frac{B_k \Delta_k}{1 + B_k \Delta_k} \right) \log_2(e) = 0,
 \end{aligned} \tag{27}$$

where $\Delta_k = \alpha_0 / \alpha_k$. Therefore, all Δ_k s $\forall k \in \{1, 2, \dots, K\}$ can be obtained from (27). For (26), we have $T = \alpha_0 + \sum_{k=1}^K \alpha_k$. The optimal solution for pair of $(\alpha_0, \{\alpha_k\})$ can be derived as follows

$$\alpha_0 = \frac{T}{1 + \sum_{k=1}^K 1 / \Delta_k} \text{ and } \alpha_k = \frac{\alpha_0}{\Delta_k}. \tag{28}$$

Finally, optimal θ and globally optimal solution for the pair of $(\alpha_0^*, \{\alpha_k^*\})$ can be decided by adopting Dinkelbach algorithm with iterating, which is shown in Algorithm 1.

Set stop criterion ϖ and **Initialize** $\theta_i=0$ for step $i=0$.

- 1: Solve (20) to obtain $(\alpha_0, \{\alpha_k\})$.
- 2: **if** $F(\theta_{i-1}) > \varpi$, **then**
- 3: Obtain $\theta_i = R_{sum,i-1} / E_{T,i-1}$ and Let $i = i + 1$, repeat 1.
- 4: **else**
- 5: Obtain $\theta_i = R_{sum,i-1} / E_{T,i-1}$ and Let $i = i + 1$.
- 6: Solve (20) to obtain globally optimal solution $(\alpha_0^*, \{\alpha_k^*\})$
- 7: **end if**

Algorithm 1 Optimal Time Allocation

5 Numerical results

In this section, we present some simulation results to verify the accuracy of the theoretical analyses and demonstrate the availability for the proposed optimal time allocation algorithm. Table 1 lists the necessary parameters for numerical results.

5.1 Beam outage probability

Figure 3 depicts the beam outage probability versus the transmit SNR of HAP for various target rates. With the increase of the transmit SNR of the HAP, the beam outage probability of the system is improved because the sensors in the service sector can harvest more energy for data transmission. In addition, a higher target rate will result in a higher beam outage probability since the links are more difficult to satisfy the transmission requirement. All analytical results are in good agreement with the Monte Carlo simulations, which verify the accuracy of the derived expression.

Figure 4 illustrates the beam outage probability with respect to the transmit SNR of HAP for the different values of central angles δ . Similar to the previous analysis, with the increase of the HAP's transmit SNR, the beam outage performance can be improved. It can be seen from the figure that the beam outage probability is decreased with a small value of central angle δ , which is due to the fact that the sensors can obtain larger channel gains in a narrower sector as they are closer to the normalized direction $\bar{\delta}$ of HAP. Furthermore, the exact analytical results are well aligned with the simulation results.

Table 1 Lists of necessary parameters

Symbol	Name	Value
R	Radius of disc	10 m
M	Number of antennas	16
λ	Density	1
δ	Central angle	0.2
Ω	Channel average power	1
α_0	Sub-interval of WEH	0.5
β	Path loss exponent	2
$P_{\text{HAP}}/\sigma_0^2$	Transmit SNR at HAP	-10 dB
η	Energy conversion efficiency	0.8

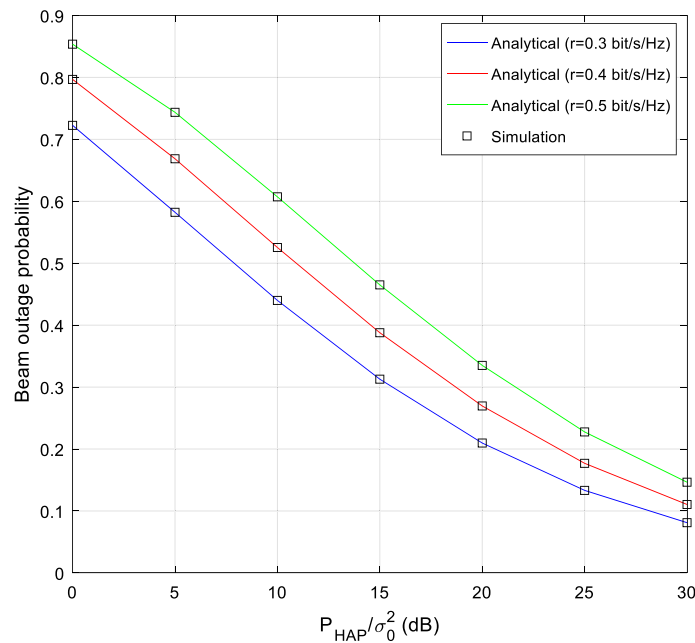


Fig. 3 Beam outage probability versus HAP's transmit SNR for different target rates

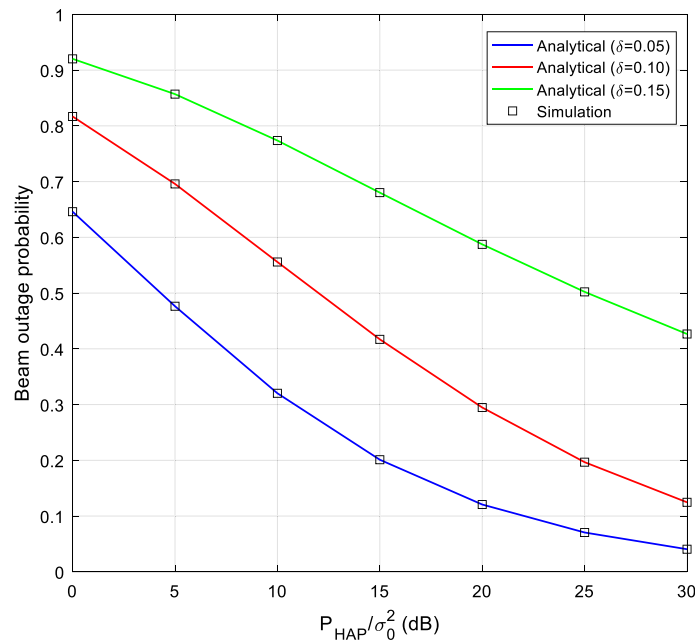


Fig. 4 Beam outage probability versus HAP's transmits SNR for different central angles

In Fig. 5, we investigate the beam outage probability versus the number of antennas at the HAP for different value of δ . We can further insight that the central angle δ significantly affects the outcome of beam outage probability by increasing the number of HAP's antennas. For small δ , the beam outage probability is first decreased and then increased to a certain value with an increase of M . This is due to fact that when the number of antennas is increased, the beam formed by the antenna can adequately

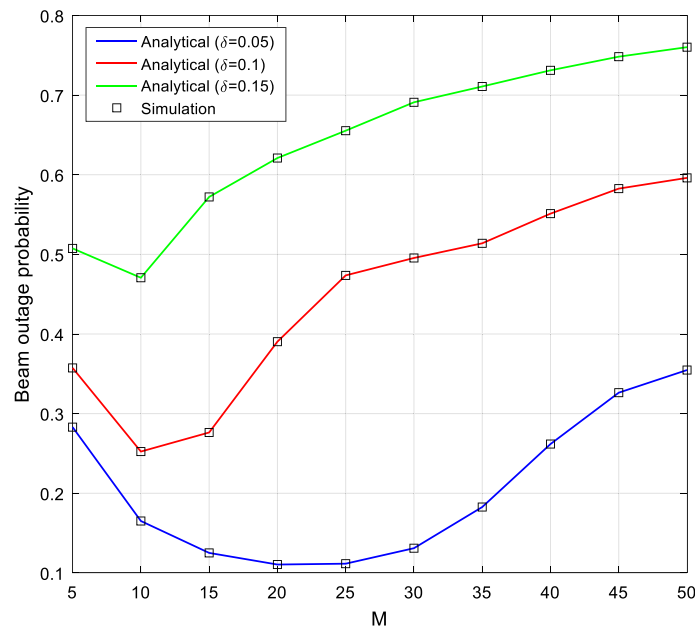


Fig. 5 Beam outage probability versus the number of antennas at the HAP for different central angles

cover the sensors in the service sector. However, if the number of antennas continues to increase, even if the generated beamforming can provide more energy to the sensors, the beamwidth will become narrow and can only serve sensors close to the normalized direction. Therefore, the beam outage probability shows an upward trend. Moreover, a larger center angle implies that the HAP needs to serve a larger area. In this scenario, increasing the number of antennas will reduce the coverage of the HAP, which results the system's beam outage probability further increasing. For a service sector with large central angle in mmWave communication systems, the more the antennas, the narrower the beamwidth, which will reduce the number of served sensors and beam outage performance. In contrast, a small number of antennas can achieve a relatively better beam outage performance. The analytical results also coincide exactly with simulation results.

Figure 6 demonstrates the beam outage probability with respect to WEH sub-interval α_0 . From the general trend, with the increase of α_0 , the system's beam outage probability first decreases and then increases. This is due to the sensors being able to harvest more RF energy with the increase of α_0 , which can improve the data transmission rate and beam outage probability to some extent. If α_0 is too long, the sub-interval for data transmission will be reduced and the beam outage performance would suffer significantly. As expected, a higher HAP's transmit power can deliver more RF energy for the sensors at a given WEH sub-interval, thus reducing the beam outage probability of the system. Meanwhile, the beam outage performance of the system decreases with the increase of the density λ , which because that the TDMA scheme is utilized so that each sensor will be allocated less WIT sub-interval as the number of sensors increases. Similarly, the numerical results agree well with the simulation results.

Figure 7 plots the system's beam outage probability versus target rates for different central angles δ . As the target rate increases, the probability that the HAP can successfully decode data will be decreased, so that the beam outage probability increases.

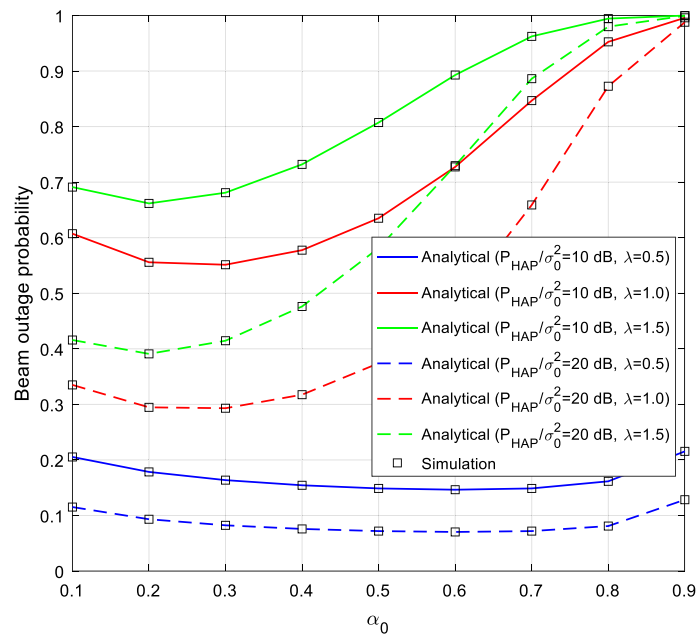


Fig. 6 Beam outage probability versus WEH sub-interval for different HAP's transmit SNRs and various density of HPPP

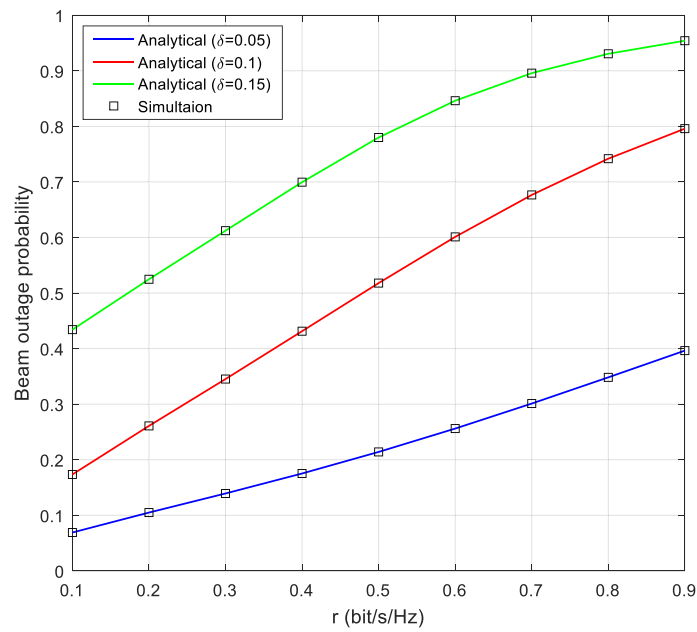


Fig. 7 Beam outage probability versus target rate for different central angles

As expected, within a smaller coverage range, the sensors will be located closer to the center angle, so that the sensors can receive energy and transmit data more effectively. As can be seen, the simulation points are perfectly aligned with the corresponding analytical curves.

5.2 Energy efficiency analysis

In this subsection, we demonstrate the energy efficiency (EE) of the system and the sum achievable rates with proposed algorithm, which are also compared to the ergodic EE and achievable sum-rate in [45].

Figure 8 depicts the changes of system’s EE and sum achievable rate versus HAP’s transmit SNR for different numbers of sensors. As can be seen from the figure, with the increase of HAP’s transmit SNR, the sum achievable rate of the system gradually increases, while the EE is gradually decreased. This is because although the sum achievable rate of the sensors in uplink transmission is improved, the correspondingly consumed energy consumed is also increased, which ultimately results in a decrease of the system’s EE. In the meanwhile, with the increase of the number of sensors, the considered HTT transmission protocol can provide WEH and WIT services for more sensors, but the timeslot allocations of energy harvesting and the data transmission will be decreased, thus reducing both the EE and sum achievable rate reachability of the system. In addition, compared with the ergodic performance analysis of the multi-user uplink transmission mmWave WPCN system considered in [45], both the EE and sum achievable rate of the system can be concurrently improved by proposed jointly optimizing the uplink and downlink transmission timeslot allocations. For example, it can be calculated from the figure that when $K=7$, compared with the comparison scheme [45], the proposed optimal timeslot allocation algorithm can increase the sum achievable rate and EE of the system by up to 25% and 26.4%, respectively.

In Fig. 9, the EE and sum achievable rates are evaluated versus HAP’s transmit SNR for different center angles. Similar to the analysis of Fig. 8, with the increase of HAP’s transmit SNR, the sum achievable rate of the system is increased, while the EE is decreased. The figure also shows that the value of center angle δ has a great impact on the system’s performance. When δ is small, the sensors are more concentrated in the near of the

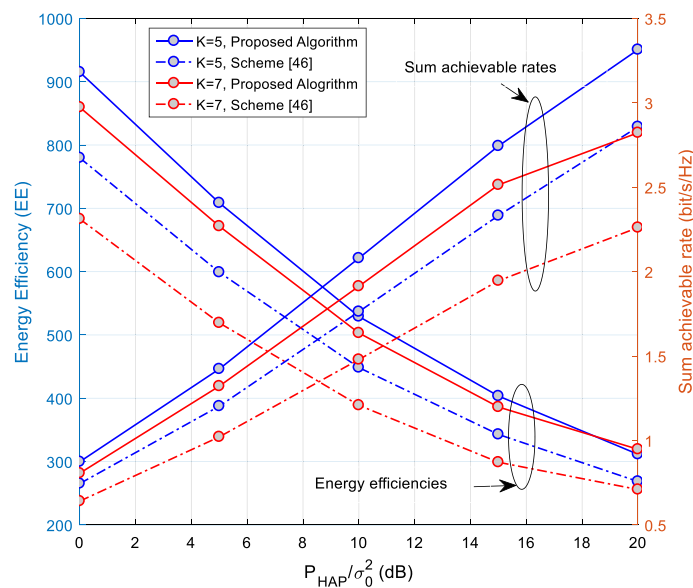


Fig. 8 Energy efficiency and sum achievable rate versus HAP’s transmit SNR for different numbers of sensors

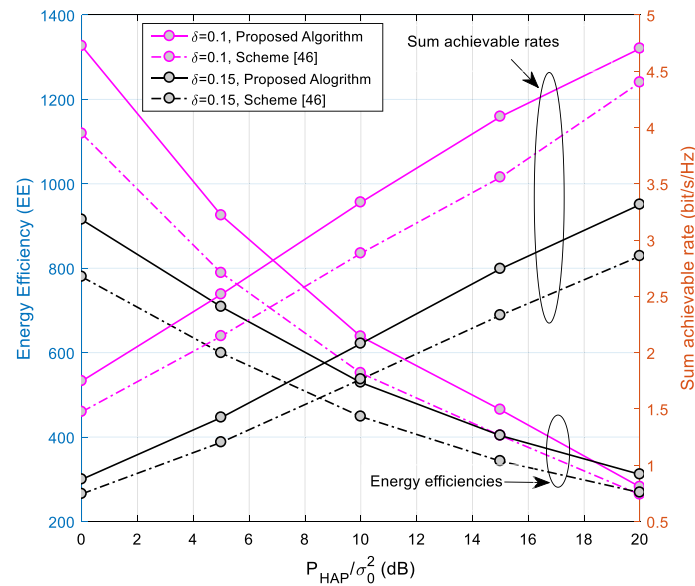


Fig. 9 Energy efficiency and sum achievable rate versus HAP's transmit SNR for different central angles

HAP's normalized direction of energy beam, so that the sensors in the service sector can harvest more energy during WEH phase for future WIT, which can promote the system sum achievable rate. Likewise, compared with ergodic performance analysis in [45], both the sum achievable rate and EE based on the proposed timeslot allocation algorithm can be maximized by 12% and 13.8%, respectively, when taking $\delta=0.1$ as an example.

6 Conclusion and discussion

In this paper, we investigate a typical wireless-powered mmWave sensor network, where a transmission interval is divided in to two sub-intervals. For the first sub-interval, a hybrid access point utilizes energy beamforming to simultaneously power the sensors within the service sector. During the remaining sub-interval, sensors transmit their data to HAP successively by using the harvested energy. According to the stochastic geometry theory, the exact expression of the system's beam outage probability is derived. The approximately closed-form expressions of beam outage probability are obtained based on some reasonable assumptions. Then, in order to maximize the system's energy efficiency, an optimal time allocation algorithm is proposed. The optimization problem can be solved by a proposed Dinkelbach algorithm, which includes parametric form transforming and KKT conditions. Extensive simulation results reveal that system's parameters significantly affect the beam outage probability, while our proposed algorithm can improve the system's energy efficiency and sum achievable rate compared to the corresponding ergodic analyses.

On the basis of this paper, in the future, we continue to carry out further in-depth research, where a mmWave-based wireless-powered communication network will be considered with combination of TDMA and FDMA operations. In order to improve the energy efficiency of the system, a joint optimization problem of multiple resource allocation is investigated and a two-stage design method is proposed to obtain optimal

resource allocation, which includes sensor grouping, antenna allocation, transmission timeslot allocation, and bandwidth allocation.

Appendix

Proof of Lemma 1 The CDF of achievable rate for a typical sensor at the HAP can be written as $\Pr \{v < r\}$. In addition, we assume that there is reciprocity between channels \mathbf{h}_k and \mathbf{h}'_k [46]. Let $X = |g|^2$, which is exponential-distributed random variable with PDF $g_X(x)$ shown as follows

$$g_X(x) = \frac{1}{\Omega} \exp\left(-\frac{x}{\Omega}\right), \tag{29}$$

where Ω denotes channel average power. Substituting (8) into (9), we thus have

$$\begin{aligned} \Pr \{v < r\} &= \Pr \left\{ \frac{\alpha_0 \eta P_{HAP} (F_M(\phi))^2}{\alpha_k \sigma_0^2 (1 + d^\beta)^2} |g|^4 < 2^{\frac{rK}{1-\alpha_0}} - 1 \right\} \\ &= \Pr \left\{ -\sqrt{2^{\frac{rK}{1-\alpha_0}} - 1} < \sqrt{\frac{\alpha_0 \eta P_{HAP}}{\alpha_k \sigma_0^2}} \frac{F_M(\phi)}{(1 + d^\beta)} |g|^2 < \sqrt{2^{\frac{rK}{1-\alpha_0}} - 1} \right\} \\ &\stackrel{(a)}{=} \Pr \left\{ 0 \leq \sqrt{\frac{\alpha_0 \eta P_{HAP}}{\alpha_k \sigma_0^2}} \frac{F_M(\phi)}{(1 + d^\beta)} |g|^2 < \sqrt{2^{\frac{rK}{1-\alpha_0}} - 1} \right\}. \end{aligned} \tag{30}$$

where (a) follows the fact that $|g|^2 \geq 0$. Then, (30) can be further written as

$$\begin{aligned} \Pr \{v < r\} &= 1 - \mathbb{E}_\Phi \left\{ \int_0^{\frac{A(1+r^\beta)}{F_M(\phi)}} g_X(x) dx \right\} \\ &\stackrel{(b)}{=} 1 - \mathbb{E}_\Phi \left\{ \exp\left(-\frac{A(1+r^\beta)}{\Omega F_M(\phi)}\right) \right\} \\ &\stackrel{(c)}{=} 1 - \int_{-\delta}^\delta \int_0^R \exp\left(-\frac{A(1+r^\beta)}{\Omega F_M(\phi)}\right) r f_d(r) dr d\phi, \end{aligned} \tag{31}$$

where $A = \sqrt{(1 - \alpha_0) \sigma_0^2 [2^{rK/(1-\alpha_0)} - 1]} / (K \alpha_0 \eta P_{HAP})$, (b) follows from the fact that $|g|^2$ is exponential distribution, (c) follows by considering the spatial distribution over all possible distances and angles. Moreover, the K sensors are deployed in service sector following HPPP and they are independently and identically distributed (i.i.d) points. Therefore, the PDF of distance for sensors can be obtained as

$$f_d(r) = \frac{\lambda}{\delta R^2 \lambda} = \frac{1}{\delta R^2}. \tag{32}$$

By substituting (31) into (30), the result of (30) can be rewritten as

$$\Pr \{v < r\} = 1 - \frac{1}{\delta R^2} \int_{-\delta}^\delta \int_0^R \exp\left(-\frac{A(1+r^\beta)}{\Omega F_M(\phi)}\right) r dr d\phi. \tag{33}$$

Abbreviations

mmWave	Millimeter-wave
WET	Wireless energy transfer
HAP	Hybrid access point
TDMA	Time-division multiple access
KKT	Karush–Kuhn–Tucker
WSN	Wireless sensor network
IoT	Internet of things
RF	Radio frequency
MIMO	Multiple-input-multiple-output
WPCN	Wireless-powered communication network
HTT	Harvest-then-transmit
WIT	Wireless information transmission
PS	Power-splitting
TS	Time-switching
OFDM	Orthogonal-frequency-division-multiple
AF	Amplify-and-forward
PB	Power beacon
SWIPT	Simultaneous wireless information and power transfer
HPPP	Homogeneous Poisson point process
LOS	Line-of-sight
NLOS	Non-line-of-sight
CDF	Cumulative distribution function
SNR	Signal-noise-ratio
EE	Energy efficiency

Acknowledgements

Not applicable.

Author contributions

XL is responsible for writing and revising the paper. FX and EL are responsible for interrupt probability analysis and simulation. KT is responsible for proposing the research objectives, methods and finalization of the paper.

Funding

This work was supported by the Natural Science Foundation of Hunan Province under Grant No. 2020JJ2015 and Grant No. 2021JJ30294 and Scientific Research Foundation of Hunan Provincial Education Department under Grant No. 22A0579, in part by the National Natural Science Foundation of China under Grant No. 61931009, Grant No. 62172159, and Grant No. 62231014. All funding agencies provides funds for the publication of the articles and for the purchase of the equipment and software required for the simulation.

Availability of data and materials

The datasets used and/or analyzed during the current study are available from the corresponding author on reasonable request.

Declarations

Ethics approval and consent to participate

Not applicable.

Consent for publication

Not applicable.

Competing interests

The authors declare that they have no competing interests.

Received: 25 July 2023 Accepted: 12 December 2023

Published online: 02 January 2024

References

1. N.T. Nguyen, B.H. Liu, V.T. Pham, C.Y. Huang, Network under limited mobile devices: a new technique for mobile charging scheduling with multiple sinks. *IEEE Syst. J.* **12**(3), 2186–2196 (2018)
2. C. Wang, J. Li, Y. Yang, F. Ye, Combining solar energy harvesting with charging for hybrid wireless sensor networks. *IEEE Trans. Mob. Comput.* **17**(3), 560–576 (2018)
3. H. Zhang, Y.X. Guo, Z. Zhong, W. Wu, Cooperative integration of RF energy harvesting and dedicated WPT for wireless sensor networks. *IEEE Microw. Wirel. Compon. Lett.* **29**(4), 291–293 (2019)
4. K. Tang, S. Liao, Q. Xue, Cooperative spectrum sharing in spectrum domain with discrete time energy harvesting for primary user. *Ad Hoc Netw.* **116**, 102474 (2021)
5. D. Newell, M. Duffy, Review of power conversion and energy management for low-power, low-voltage energy harvesting powered wireless sensors. *IEEE Trans. Power Electron.* **34**(10), 9794–9805 (2019)

6. J. Hu, J. Luo, Y. Zheng, K. Li, Graphene-grid development in energy harvesting cooperative wireless sensor networks for green IoT. *IEEE Trans. Industr. Inf.* **15**(3), 1820–1829 (2019)
7. A. Riaz, S. Zakir, M.M. Farooq, M. Awais, W.T. Khan, A tri-band rectifier toward millimeter-wave frequencies for energy harvesting and wireless power-transfer applications. *IEEE Microw. Wirel. Compon. Lett.* **31**(2), 192–195 (2021)
8. X. Lu, P. Wang, D. Niyato, D.I. Kim, H. Zhu, Wireless networks with RF energy harvesting: a contemporary survey. *IEEE Commun. Surv. Tutor.* **17**(2), 757–789 (2015)
9. J. Kim, B. Clerckx, Range expansion for wireless power transfer using joint beamforming and waveform architecture: an experimental study in indoor environment. *IEEE Wirel. Commun. Lett.* **10**(6), 1237–1241 (2021)
10. S. Bi, C.K. Ho, R. Zhang, Wireless powered communications: Opportunities and challenges. *IEEE Commun. Mag.* **53**(4), 117–125 (2015)
11. Z. Lin, H. Niu, K. An, Y. Wang, G. Zheng, S. Chatzinotas, Y. Hu, Refracting RIS-aided hybrid satellite-terrestrial relay networks: joint beamforming design and optimization. *IEEE Trans. Aerosp. Electron. Syst.* **58**(4), 3717–3724 (2022)
12. S. Mumtaz, J. Rodriguez, L. Dai, *MmWave Massive MIMO: A Paradigm for 5G* (Academic, New York, 2016)
13. S.A. Busari, K.M.S. Huq, S. Mumtaz, L. Dai, J. Rodriguez, Millimeter-wave massive MIMO communication for future wireless systems: a survey. *IEEE Commun. Surv. Tutor.* **20**(2), 836–869 (2018)
14. W. Roh, J.Y. Seol, J. Park, B. Lee, J. Lee, Y. Kim, J. Cho, K. Cheun, F. Aryanfar, Millimeter-wave beamforming as an enabling technology for 5G cellular communications: theoretical feasible and prototype results. *IEEE Commun. Mag.* **52**(2), 106–113 (2014)
15. G.N. Kamga, S. Aissa, Wireless power transfer in mmWave massive MIMO systems with/without rain attenuation. *IEEE Trans. Commun.* **67**(1), 176–189 (2019)
16. P. Ramezani, A. Jamalipour, Optimal resource allocation in backscatter assisted WPCN with practical energy harvesting model. *IEEE Trans. Veh. Technol.* **68**(12), 12406–12410 (2019)
17. A. Li, C. Masouros, Energy-efficient SWIPT: from fully digital to hybrid analog-digital beamforming. *IEEE Trans. Veh. Technol.* **67**(4), 3390–3405 (2018)
18. O. Rezaei, M.M. Naghsh, Z. Rezaei, R. Zhang, Throughput optimization for wireless powered interference channels. *IEEE Trans. Wirel. Commun.* **18**(5), 2464–2476 (2019)
19. G. Kwon, H. Park, M.Z. Win, Joint beamforming and power splitting for wideband millimeter wave SWIPT systems. *IEEE J. Sel. Top. Signal Process.* **15**(5), 1211–1227 (2021)
20. W. Lu, P. Si, G. Huang, L. Qian, N. Zhao, Y. Gong, SWIPT cooperative spectrum sharing for 6G-enabled cognitive IoT networks. *IEEE Internet Things J.* **8**(20), 15070–15080 (2021)
21. Z. Lin, M. Lin, T.D. Cola, J.-B. Wang, W.-P. Zhu, J. Cheng, Supporting IoT with rate-splitting multiple access in satellite and aerial-integrated networks. *IEEE Internet Things J.* **8**(14), 11123–11134 (2021)
22. Z. Wang, Z. Chen, B. Xia, L. Luo, J. Zhou, Cognitive relay networks with energy harvesting and information transfer: design, analysis, and optimization. *IEEE Trans. Wirel. Commun.* **15**(4), 2562–2576 (2016)
23. J. Ye, Z. Liu, H. Zhao, G. Pan, Q. Ni, M.-S. Alouini, Relay selections for cooperative underlay CR systems with energy harvesting. *IEEE Trans. Commun. Netw.* **5**(2), 358–369 (2019)
24. A. Sirojuddin, W.-J. Huang, Sum-rate maximization in two-way MIMO cooperative networks with an energy harvesting relay. *IEEE Trans. Wirel. Commun.* **21**(6), 3664–3677 (2022)
25. Y. Yao, Z. Ni, W. Hu, M. Motani, Optimizing energy harvesting decode-and-forward relays with decoding energy costs and energy storage. *IEEE Access* **9**, 96613–96628 (2021)
26. W. Lu, Y. Gong, X. Liu, J. Wu, H. Peng, Collaborative energy and information transfer in green wireless sensor network for smart cities. *IEEE Trans. Ind. Inf.* **14**(4), 1585–1593 (2018)
27. Z. Lin, M. Lin, J.-B. Wang, T.D. Cola, J. Wang, Joint beamforming and power allocation for satellite-terrestrial integrated networks with non-orthogonal multiple access. *IEEE J. Sel. Top. Signal Process.* **13**(3), 657–670 (2019)
28. T.X. Tran, W. Wang, S. Luo, K.C. The, Nonlinear energy harvesting for millimeter wave networks with large-scale antennas. *IEEE Trans. Veh. Technol.* **67**(10), 9488–9498 (2018)
29. T.A. Khan, R.W. Heath Jr., Wireless power transfer in millimeter wave tactical networks. *IEEE Signal Process. Lett.* **24**(9), 1284–1287 (2017)
30. J. Guo, X. Zhou, S. Durrani, Wireless power transfer via mmWave power beacons with directional beamforming. *IEEE Wirel. Commun. Lett.* **8**(1), 17–20 (2019)
31. Y. Liang, Y. He, J. Qiao, Optimal power splitting for simultaneous wireless information and power transfer in millimeter-wave networks, *IEEE Conference on Computer Communications Workshops*, pp. 1117–1122, 2020 (2020)
32. A.N. Uwaechia, N.M. Mahyudin, Spectrum and energy efficiency optimization for hybrid precoding-based SWIPT-enabled mmWave mMIMO-NOMA systems. *IEEE Access* **8**, 139994–140007 (2020)
33. X. Sun, W. Yang, Y. Cai, L. Tao, Y. Liu, Y. Huang, Secure transmissions in wireless information and power transfer millimeter-wave ultra-dense networks. *IEEE Trans. Inf. Forensics Secur.* **14**(7), 1817–1829 (2019)
34. Z. Lin, K. An, H. Niu, Y. Hu, S. Chatzinotas, G. Zheng, J. Wang, SLNR-based secure energy efficiency beamforming in multibeam satellite systems, *IEEE Trans. Aerosp. Electron. Syst. Early Access* (2022). <https://doi.org/10.1109/TAES.2022.3190238>
35. Z. Lin, B. Champagne, W.-P. Zhu, N. Al-Dhahir, Secrecy-energy efficient hybrid beamforming for satellite-terrestrial integrated networks. *IEEE Trans. Commun.* **69**(9), 6345–6360 (2021)
36. Z. Lin, K. An, H. Niu, Y. Hu, S. Chatzinotas, G. Zheng, J. Wang, SLNR-based secure energy efficient beamforming in multibeam satellite systems. *IEEE Trans. Aerosp. Electron. Syst.* **59**(2), 2085–2088 (2023)
37. H. Wang, D.G. Fang, M. Li, A single-channel microstrip electronic tracking antenna array with time sequence phase weighting on sub-array. *IEEE Trans. Microw. Theory Tech.* **58**(2), 253–258 (2010)
38. M.R. Akdeniz, Y. Liu, M.K. Samimi et al., Millimeter wave channel modeling and cellular capacity evaluation. *IEEE J. Sel. Areas Commun.* **32**(6), 1164–1179 (2014)
39. G. Lee, Y. Sung, J. Seo, Randomly-directional beamforming in millimeter-wave multiuser MISO downlink. *IEEE Trans. Wireless Commun.* **15**(2), 1086–1100 (2016)
40. Z. Ding, P. Fan, H.V. Poor, Random beamforming in NOMA networks. *IEEE Access* **5**, 7667–7681 (2017)

41. Y. Zeng, B. Clerckx, R. Zhang, Communications and signals design for wireless power transmission. *IEEE Trans. Commun.* **65**(5), 2264–2290 (2017)
42. T. Lv, Y. Ma, J. Zeng et al., Millimeter-wave NOMA transmission in cellular M2M communications for internet of things. *IEEE Internet Things J.* **5**(3), 1989–2000 (2018)
43. X. Luo, H. Zhu, IRS-based TDMA reciprocity breaking for pilot decontamination in massive MIMO. *IEEE Wirel. Commun. Lett.* **10**(1), 102–106 (2020)
44. S. Boyd, L. Vandenberghe, *Convex Optimization* (Cambridge University Press, New York, 2004)
45. J.C. Guo, Q.Y. Yu, W.X. Meng, M. Xiang, Ergodic energy efficiency of mmWave system considering insertion loss under dynamic subarray architecture, in *IEEE Vehicular Technology Conference* (2020)
46. X. Jiang, F. Kaltenberger, Channel reciprocity calibration in TDMA hybrid beamforming massive MIMO systems. *IEEE J. Sel. Top. Signal Process.* **12**(3), 422–431 (2018)

Publisher's Note

Springer Nature remains neutral with regard to jurisdictional claims in published maps and institutional affiliations.

Submit your manuscript to a SpringerOpen[®] journal and benefit from:

- ▶ Convenient online submission
- ▶ Rigorous peer review
- ▶ Open access: articles freely available online
- ▶ High visibility within the field
- ▶ Retaining the copyright to your article

Submit your next manuscript at ▶ [springeropen.com](https://www.springeropen.com)
